Analysis, simulation and relative performances of two kinds of serpentine springs

INSTITUTE OF PHYSICS PUBLISHING JOURNAL OF MICROMECHANICS AND MICROENGINEERING

J. Micromech. Microeng. **15** (2005) 736–746 doi:10.1088/0960-1317/15/4/010

Analysis, simulation and relative performances of two kinds of serpentine springs

Giuseppe Barillaro[1], **Antonio Molfese**[1,2], **Andrea Nannini**[1] and **Francesco Pieri**[1]

[1] Dipartimento di Ingegneria dell'Informazione, Università di Pisa, Italy
[2] Istituto di Elettronica e di Ingegneria dell'Informazione e delle Telecomunicazioni, C.N.R., Sezione di Pisa, Italy

E-mail: antonio.molfese@iet.unipi.it

Received 23 July 2004, in final form 3 December 2004
Published 14 February 2005
Online at stacks.iop.org/JMM/15/736

Abstract

A complete set of approximate, closed-form expressions, obtained with small displacements theory, for the spring constants of two kinds of serpentine springs (classic and rotated) is presented. The expressions are proposed as a tool for rapid design of microelectromechanical structures. The two designs are also studied numerically using the finite element method (FEM): analytical calculations and FEM simulations are compared. A comparison between the performances of the two designs is also briefly presented.

Table 1. Nomenclature.

Symbol	Definition
A	Beam or spring cross-section (m^2)
E	Young's modulus (Pa)
F_i	Force parallel to the i-axis (N)
G	Shear modulus equal to $E/(2(1+\nu))$ (Pa)
I_{y_o}	Moment of inertia with respect to the y-axis of the section of the element of the spring orthogonal to the x and z axes (m^4)
I_{y_p}	Moment of inertia with respect to the y-axis of the section of the element of the spring parallel to the x-axis (m^4)
I_{z_o}	Moment of inertia with respect to the z-axis of the section of the spring element orthogonal to the x and z axes (m^4)
I_{z_p}	Moment of inertia with respect to the z-axis of the section of the spring element parallel to the x-axis (m^4)
$K^C_{\delta_y}$, $K^R_{\delta_y}$	Spring constant F_y/Δ_y with guided end, for a classic and for a rotated serpentine spring, respectively (N m^{-1})
$K^C_{\delta_z}$, $K^R_{\delta_z}$	Same as above for spring constant F_z/Δ_z with guided end (N m^{-1})
K_i	Spring constant F_i/δ_i (N m^{-1})
K_{ij}	Spring constant F_j/δ_i (N m^{-1})
$K_{i\theta_j}$	Spring constant M_j/Δ_i (N)
K_{θ_i}	Spring constant M_i/θ_i (N m)
$K_{\theta_i j}$	Spring constant F_j/θ_i (N)
$K_{\theta_i\theta_j}$	Spring constant M_j/θ_i (N m)
K^C_x, K^R_x	Spring constant F_x/Δ_x, for a classic and for a rotated serpentine spring, respectively (N m^{-1})
K^C_y, K^R_y	Same as above for spring constant F_y/Δ_y (N m^{-1})
K^C_z, K^R_z	Same as above for spring constant F_z/Δ_z (N m^{-1})
$K^C_{z\theta_y}$, $K^R_{z\theta_y}$	Same as above for spring constant M_y/Δ_z (N)
$K^C_{\theta_x}$, $K^R_{\theta_x}$	Same as above for spring constant M_x/θ_x (N m)
$K^C_{\theta_y}$, $K^R_{\theta_y}$	Same as above for spring constant M_y/θ_y (N m)
$K^C_{\theta_z y}$, $K^R_{\theta_z y}$	Same as above for spring constant F_y/θ_z (N)
$K^C_{\theta_z}$, $K^R_{\theta_z}$	Same as above for spring constant M_z/θ_z (N m)
J_o	Cross-sectional torsion factor the spring element orthogonal to the x- and z-axes (m^4)
J_p	Cross-sectional torsion factor of the spring element parallel to the x-axis (m^4)
l_o	Length of the spring element orthogonal to the x- and z-axes (m)
l_p	Length of the spring element parallel to the x-axis (m)
M_i	Torsion moment or torque around the i-axis (N m)
N	Number of foldings (−)
t	Thickness of the structural layer (m)

Table 1. (Continued.)

Symbol	Definition
w_o	Width of the spring element orthogonal to the x- and z-axes (m)
w_p	Width of the spring elements parallel to the x-axis (m)
ν	Poisson's ratio (−)

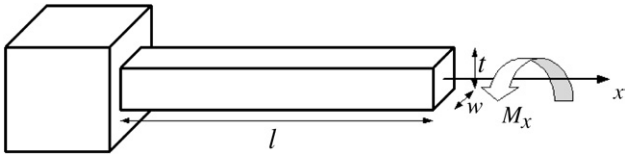

Figure 1. Torsion bar.

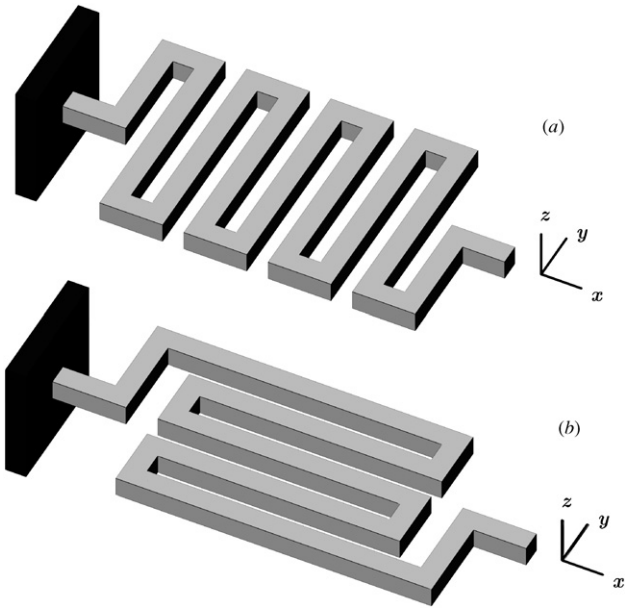

Figure 2. Classic serpentine spring (a); rotated serpentine spring (b).

1. Introduction

Among the most important steps in the development of a new MEMS device is the design of each element of the involved mechanical structures through tools that allow rapid prototyping and optimization of the relevant design parameters (e.g., stiffness, occupation of area, forces, capacitances, etc). To this purpose, the value to the designer of analytical expressions for the physical features of the structures, which allow optimization of the parameters before simulation, should not be underestimated.

Springs are among the most important elements in MEMS devices. Several different kinds of springs were presented in the literature [1], all of them with advantages and drawbacks for a particular application. An interesting case is constituted by serpentine springs, getting their name from the meandering snake-like pattern of the spring segment [1]. They are used in several applications: accelerometers, resonators, etc. Although they are more commonly used to perform in-plane displacements, they can also be used for out-of-plane displacements, and angular deflections (i.e. as torsional springs) as well [2–7], where they allow small spring constants with a reasonable occupation of area.

The main feature of several surface MEMS processes [7, 8], among them, for example, the one developed at Robert Bosch GmbH [8], is the presence of a thick structural polysilicon layer; for this kind of process the classic torsional spring, made as a simple straight bar and shown in figure 1, does not allow for low torsional spring constants because of the thickness of the structural layer. A possible solution is the use of *serpentine springs*.

This kind of spring, apart from reducing the occupied area for the same spring constant, has the advantage of solving the problem of the buckling produced by the residual stress [2]. It was also shown that by using serpentine torsional springs the resonance frequencies are completely independent of the residual stress value, while there is a large dependence for simple straight torsional rods with similar torsional spring constants [9].

The shape of this kind of spring is shown in figure 2(a). The reduction of the torsional stiffness is mainly due to the elements orthogonal to the torsional axis, which are subject to a bending stress. Unfortunately, as the thickness of the structural layer increases, the bending stiffness of the orthogonal elements, which is proportional to the third power of the thickness [10], rapidly becomes so high that the advantage of this type of design is almost lost.

This problem can be overcome by a 90° rotation of the spring elements around the vertical axis, obtaining the *rotated serpentine spring* (figure 2(b)) [11]. With this design, the spring elements (which are now parallel to the torsional axis) are mainly subject to torsional stress, which is approximately linearly dependent on the value of the thickness.

The aim of this paper is to convert these qualitative considerations into a quantitative analysis. To this scope, we will deduce analytical expressions for several elements of the stiffness matrix (as defined in [12]) of both spring types by using the principle of virtual work with the unit-load method [10]. The analytical results will be compared with those obtained with a finite element method (FEM) commercial software package for structural analysis.

2. Modeling and method of analysis

In order to characterize the springs we calculate the displacement Δ_i (or the rotation θ_i) resulting from a force F_j (or a torque M_j) applied in the appropriate direction, where $i, j \in \{x, y, z\}$. Only displacements from bending and torsion are considered in the analysis. Deformations from shear, compression and traction are neglected. Throughout the paper, the system of coordinates of figure 2 will be used and the springs will be oriented so as to lie in the xy-plane with the main axis parallel to x. The spring constant is defined as $K_{ij} = F_j/\delta_i$ (or $K_{\theta_i\theta_j} = M_j/\theta_i$). To simplify notation, if the two subscripts are identical, the second will be dropped. The resulting constants can be arranged in a 6×6 spring matrix:

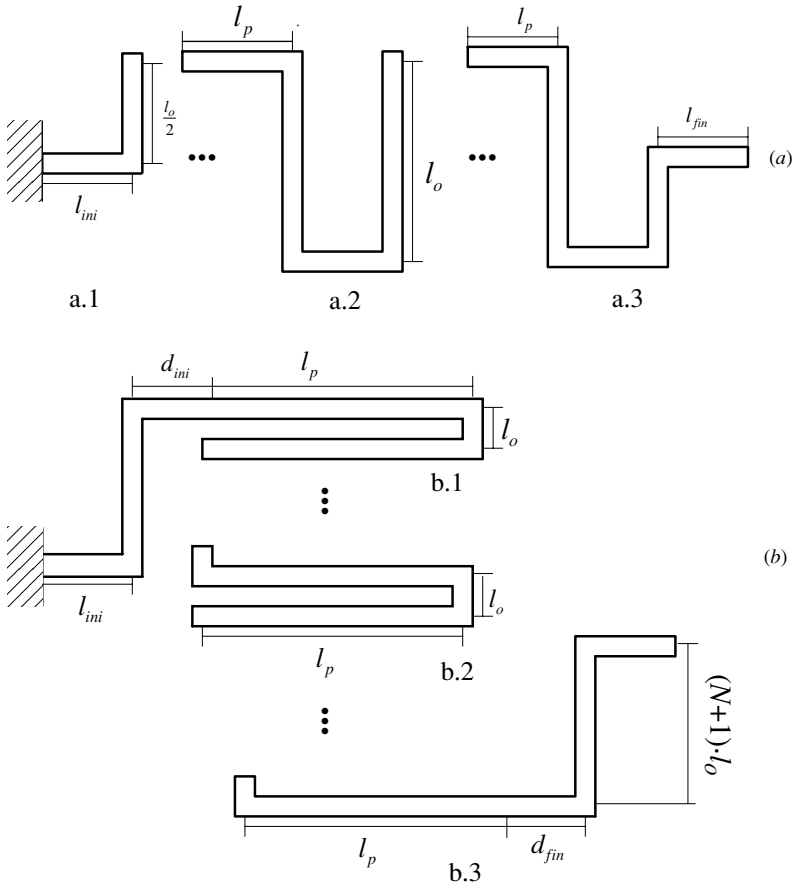

Figure 3. Design variables of serpentine springs. It is constituted by three parts: the initial (a.1 and b.1) and final parts (a.3 and b.3) used to connect it to the anchor and to the movable mass and a central part (a.2 and b.2) which can be repeated.

$$K = \begin{pmatrix} K_x & K_{xy} & K_{xz} & K_{x\theta_x} & K_{x\theta_y} & K_{x\theta_z} \\ K_{yx} & K_y & K_{yz} & K_{y\theta_x} & K_{y\theta_y} & K_{y\theta_z} \\ K_{zx} & K_{zy} & K_z & K_{z\theta_x} & K_{z\theta_y} & K_{z\theta_z} \\ K_{\theta_x x} & K_{\theta_x y} & K_{\theta_x z} & K_{\theta_x} & K_{\theta_x\theta_y} & K_{\theta_x\theta_z} \\ K_{\theta_y x} & K_{\theta_y y} & K_{\theta_y z} & K_{\theta_y\theta_x} & K_{\theta_y} & K_{\theta_y\theta_z} \\ K_{\theta_z x} & K_{\theta_z y} & K_{\theta_z z} & K_{\theta_z\theta_x} & K_{\theta_z\theta_y} & K_{\theta_z} \end{pmatrix}.$$

This matrix is symmetric, and has only 21 independent terms. The number of independent nonzero terms reduces to 12 assuming there are no variations in geometry along the z-direction and therefore, no coupling between in-plane and out-of-plane directions [12]. The expressions for some of the elements of this matrix for serpentine springs were already presented [1, 12], but the problem of the torsional spring constant K_{θ_x} has not been completely analyzed.

The elements of the spring constants matrix are calculated by using the principle of virtual work with the unit-load method, as detailed in appendix A.

The two types of springs (serpentine and rotated serpentine) are parametrized as shown in figure 3. The classic serpentine springs are divided into three parts (figure 3). The first (a.1) and the third (a.3) are used to connect the spring to the anchor and to the movable mass and to make the architecture symmetric. The second part is constituted by N repeated elements of the type (a.2). The rotated serpentine springs are divided in a similar way (figure 3). In order to simplify the calculation we suppose $l_{\text{ini}} = l_{\text{fin}} = l_{\text{p}}$ and $d_{\text{ini}} = d_{\text{fin}} = d_{\text{p}}$ in all our analyses.

We analyze the behavior of the springs in the case of arbitrary N. Every spring is analyzed as the connection of several elementary beams, each one withstanding torsion and bending deformation. The length of each beam is measured along the central axis of the beam, between the centers of two consecutive corners (see figure 3). We also suppose the joints are ideal, i.e. they transfer the forces and torques without significant deformation. This is an approximation that has to be taken into account when the results of the theoretical analysis are compared with the FEM simulations of the solid model.

3. Analytical expressions for the spring constants

Following the approach sketched out in the preceding section, we computed analytical expressions for the most interesting spring constants of both classic and rotated serpentines, and in particular for those of interest in applications where a torsional spring is required. To allow a more straightforward analysis of the final expressions, the lengthy calculations required to derive such formulae were moved to appendix B. For all the following calculations the nomenclature listed in table 1 is used.

The spring constant of interest for use in torsional applications (as, e.g., those in [4, 6]) is clearly $K_{\theta_x} = M_x/\theta_x$, i.e. the constant for a torsion along the axis of the spring. The expressions for $K^{\text{C}}_{\theta_x}$ (for classic springs) and $K^{\text{R}}_{\theta_x}$ (for rotated

Table 2. Calculated spring constants of a classic serpentine spring.

Classic serpentine spring constants
$K_{\theta_x}^{\mathrm{C}} = \left[\frac{2(N+1)}{EI_{y_o}} l_o + \frac{2(N+2)}{GJ_p} l_p\right]^{-1}$
$K_{\theta_x}^{\mathrm{C}} \simeq \frac{EI_{y_o}}{2(N+1)l_o}$ (if $l_o \gg l_p$)
$K_x^{\mathrm{C}} = \left[\frac{(N+1)l_o^3}{6EI_{z_o}} + \frac{(N+1)l_o^2 l_p}{2EI_{z_p}}\right]^{-1}$
$K_x^{\mathrm{C}} \simeq \frac{6EI_{z_o}}{(N+1)l_o^3}$ (if $l_o \gg l_p$)
$K_{\delta_y}^{\mathrm{C}} = \frac{K_{y\theta_z}^{\mathrm{C}} K_{\theta_z y}^{\mathrm{C}} K_y^{\mathrm{C}}}{K_{y\theta_z}^{\mathrm{C}} K_{\theta_z y}^{\mathrm{C}} - K_y^{\mathrm{C}} K_{\theta_z}^{\mathrm{C}}}$
$K_{\delta_y}^{\mathrm{C}} \simeq \frac{3EI_{z_o}(N+1)}{(12N^4+64N^3+130N^2+116N+38)l_p^2 l_o}$ (if $l_o \gg l_p$)
$K_{\delta_z}^{\mathrm{C}} = \frac{K_{z\theta_y}^{\mathrm{C}} K_{\theta_y z}^{\mathrm{C}} K_z^{\mathrm{C}}}{K_{z\theta_y}^{\mathrm{C}} K_{\theta_y z}^{\mathrm{C}} - K_z^{\mathrm{C}} K_{\theta_y}^{\mathrm{C}}}$
$K_{\delta_z}^{\mathrm{C}} \simeq \frac{6EI_{y_o} GJ_o}{(N+1)GJ_o l_o^3 + (16N^3+36N^2+43N+3)EI_{y_o} l_p^2 l_o}$ (if $l_o \gg l_p$)

Table 3. Calculated spring constants of a rotated serpentine spring.

Rotated serpentine spring constants
$K_{\theta_x}^{\mathrm{R}} = \left[\frac{4(N+1)}{EI_{y_o}} l_o + \frac{(2N+3)l_p + 2d_p + l_{ini} + l_{fin}}{GJ_p}\right]^{-1}$
$K_{\theta_x}^{\mathrm{R}} \simeq \frac{GJ_p}{(2N+3)l_p}$ (if $l_p \gg l_o, l_{ini}, l_{fin}, d_p$)
$K_x^{\mathrm{R}} = \left[\frac{(4((N+1)l_o)^3}{3EI_{z_o}} + \frac{(2N^3+9N^2+13N^2+6)l_p + 6(N+1)d_p}{3EI_{z_p}} l_o^2\right]^{-1}$
$K_x^{\mathrm{R}} \simeq \frac{3EI_{z_p}}{(2N^3+9N^2+13N+6)l_p l_o^2}$ (if $l_p \gg l_o, l_{ini}, l_{fin}, d_p$)
$K_{\delta_y}^{\mathrm{R}} = \frac{K_{y\theta_z}^{\mathrm{R}} K_{\theta_z y}^{\mathrm{R}} K_y^{\mathrm{R}}}{K_{y\theta_z}^{\mathrm{R}} K_{\theta_z y}^{\mathrm{R}} - K_y^{\mathrm{R}} K_{\theta_z}^{\mathrm{R}}}$
$K_{\delta_y}^{\mathrm{R}} \simeq \frac{12EI_{z_p}}{(2N+3)l_p^3}$ (if $l_p \gg l_o, l_{ini}, l_{fin}, d_p$)
$K_{\delta_z}^{\mathrm{R}} = \frac{K_{z\theta_y}^{\mathrm{R}} K_{\theta_y z}^{\mathrm{R}} K_z^{\mathrm{R}}}{K_{z\theta_y}^{\mathrm{R}} K_{\theta_y z}^{\mathrm{R}} - K_z^{\mathrm{R}} K_{\theta_y}^{\mathrm{R}}}$
$K_{\delta_z}^{\mathrm{R}} \simeq \frac{12EI_{y_p}}{(2N+3)l_p^3}$ (if $l_p \gg l_o, l_{ini}, l_{fin}, d_p$ and high N)

springs) are calculated in appendix B.1 and are given in the first rows of tables 2 and 3, respectively. By analyzing the expression for $K_{\theta_x}^{\mathrm{C}}$ it is easy to recognize that the first term is contributed by the bending stiffness of the spring elements (of length l_o) orthogonal to the x-axis, while the second term is contributed by the torsional stiffness of the elements (of length l_p) parallel to the same axis. A reasonable design approach to lower $K_{\theta_x}^{\mathrm{C}}$ with a given occupied area is to make l_p much smaller than l_o, so that the second term becomes negligible. With this hypothesis, the formula simplifies to a more manageable expression, also given in table 2.

A similar analysis can be carried out for $K_{\theta_x}^{\mathrm{R}}$. With rotated springs, the orthogonal elements are again subject to bending, and the parallel ones again withstand a torsion. The expression is complicated somewhat by the presence of the connecting elements (of length d_p, l_{ini} and l_{fin}) at the beginning and end of the spring. Nevertheless, the expression can be simplified, this time by making the assumption that l_p is much bigger than l_o and the lengths of the aforementioned connecting elements, obtaining a formula which is useful for a rough estimate of spring behavior.

By substituting the expressions of I_{y_o} and J_p given in equations (B.3) and (B.4), we can compare the different

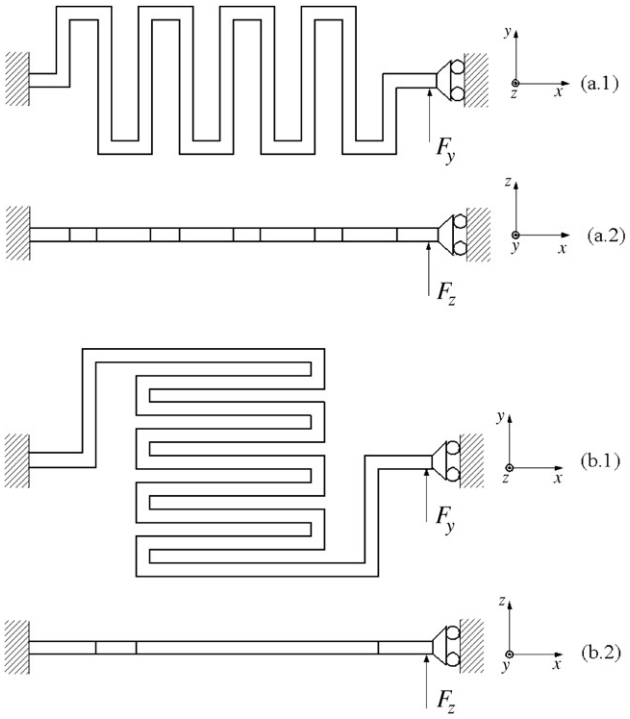

Figure 4. Classic serpentine spring with guided end along the y-axis (a.1) and along the z-axis (a.2). Rotated serpentine spring with guided end along the y-axis (b.1) and along the z-axis (b.2).

dependences of the two spring constants on the thickness value. For the classic serpentine springs $K_{\theta_x}^{\mathrm{C}}$ simply expands to

$$K_{\theta_x}^{\mathrm{C}} \simeq \frac{E w_o t^3}{24(N+1)l_o}$$

which depends on the third power of the thickness. For the rotated spring, by making the (admittedly oversimplifying) hypothesis of $t \gg w_p$, i.e. of high thickness, and thus neglecting the series in equation (B.4), we obtain

$$K_{\theta_x}^{\mathrm{R}} \simeq \frac{G t w_p^3}{3(2N+3)l_p}$$

which only depends on the first power of t. This advantage is progressively reduced for smaller and smaller thicknesses, but nonetheless confirms the qualitative considerations on the advantages of the use of rotated serpentine springs for torsional applications when a thick structural layer is available.

Apart from torsion, a very common use of these springs is as elastic elements in a linear actuator [7] or linear accelerometer [1]. A constant of interest for this case is then $K_x = F_x/\Delta x$. The expressions for K_x^{C} and K_x^{R} were thus calculated as well (appendix B.2—tables 2 and 3, second row). For this spring constant, substitution of the analytical expression of I_{z_o} and I_{z_p} results in expressions that exhibit the same (linear) dependence on the thickness.

For linear deflection along the other two axes (y and z), the most common cases in applications are such that the end of the spring is bound to move in the zy-plane without rotation, i.e. the case of *guided end* [1]. We thus define K_{δ_y} as the ratio $F_y/\Delta y$ when the spring end is bound to move along the y-axis without rotation (figure 4 (a.2, b.2)), and K_{δ_z} as the ratio $F_z/\Delta z$ when the end is bound to move along the z-axis without

Table 4. List of dimensions of the simulated springs.

	Classic serpentine	Rotated serpentine
t (μm)	5–10–15	5–10–15
N	0–3–5	0–3–5
l_p (μm)	5	20–40 $\cdots$ 200
w_p (μm)	2	2
l_o (μm)	20–40 $\cdots$ 200	5
w_o (μm)	2	2
l_{ini} (μm)	5	5
l_{fin} (μm)	5	5
d_p (μm)	5	5

rotation (figure 4 (a.1, b.1)). The full and approximated expressions for both kinds of spring are again derived in appendices B.3, B.4, B.5 and B.6 and given in tables 2 and 3, third and fourth row.

Again, an analysis of the dependence of K_{δ_y} and K_{δ_z} on the design variables can be carried out. An interesting point is that, for classic springs, they depend inversely on the fourth and third power of N, respectively, while for the rotated springs they show a linear dependence on N. When using such elements as torsional springs, highly linear K are desirable (with respect to the torsional one), because the resonance modes associated with translational degrees of freedom will be higher, thus avoiding their accidental excitation. In other words, for torsional applications, the torsional resonance frequency should be the lowest for the device. Because of the mentioned dependence of K_{δ_y} and K_{δ_z} on N, this is easier to do with the rotated type. Thus, once again, rotated springs are more suitable than classic springs for torsional applications. This last consideration shows that, regardless of the particular application, all of these constants are needed for proper design of the spring, because the target value for one of the constants (say K_{θ_x} for torsional applications) should be designed by maintaining at the same time high values for the other constants, to avoid undesired deflections of the suspended structures, as well as parasitic resonant modes at low frequencies along the same degrees of freedom.

4. FEM simulations

4.1. Description

In order to verify the analytical relationships found for the elastic spring constants we used a finite-element simulation program, ANSYS, and we implemented two kinds of simulations. The first one used the element BEAM4 to model the spring as a set of linked beams. BEAM4 [3] is a uniaxial element with tension, compression, torsion and bending capabilities. The element has six degrees of freedom at each node: displacements in the nodal x-, y- and z-directions and rotations about the nodal x-, y- and z-axes.

In the second kind of simulation, a three-dimensional meshing of the structures with the element SOLID45 (see footnote 3) was performed. SOLID45 is a brick element defined by eight nodes having three degrees of freedom (displacements) at each node. The geometrical parameters used in simulations for classic and rotated springs are listed in table 4.

[3] Documentation of Ansys Release 7.0.

4.2. Results

The results of the simulations when the beam model was used are in perfect agreement with the analytic expressions, a result that was expected as the BEAM4 is based on the elementary beam theory, used to deduce the analytical formulae as well. The very good fitting confirms the analytical relationships we found.

The results of the simulations with the solid model deviate from the analytical results. In order to compare the FEM simulations with the analytical relations we define K_{sim} and K_{cal} as the spring constant obtained respectively from the simulations and from the analytical formulae. Hence we calculate the relative error $\epsilon = (K_{sim} - K_{cal})/K_{sim}$ for both springs versus the most relevant dimension (l_o for the classic serpentine shape and l_p for the rotated serpentine shape), using the number of the repeated elements N and the thickness t as parameters.

In figure 5 the relative errors on the spring constants for the classic serpentine springs are plotted. For high thickness (15 μm) a considerable error (about 50%) is found for $K^C_{\theta_x}$. This is due to the fact that, for high thickness, the slender beam approximation for each element of the spring is not valid, so that the evaluation of the bending is not exact. A large error is also found for the elastic constants $K^C_{\delta_z}$, in which the term of the bending along the z-axis is significative, so that there is a high dependence on the thickness value. In other cases we found that the error is always under 20%.

In figure 6 the relative errors on the spring constants for the rotated serpentine springs are plotted. A large error (50%) is found for $K^R_{\delta_z}$, again because of the high value of thickness (15 μm). For K^R_x and $K^R_{\delta_y}$ the error is less than 20% and 15%, respectively. For $K^R_{\theta_x}$, the relative error is less than 20% except for low values of l_o and the thickness equal to 15 μm, when the error is more than 30%.

The differences between the calculated and simulated values could also be caused by the fact that, in the described model, the length of the beams which constitutes the spring is supposed to be equal to the distance between the centers of two consecutive corners. This is clearly an approximation, especially when the dimensions of the corners are comparable with the length of the beam. It is also supposed that the joints between the beams are ideal, but this assumption becomes less and less valid as the section of the beam (and of the joints) becomes larger, i.e. for high thickness. For all the spring constants we verified a reduction of the error for high value of the parameters l_o and l_p, which validates the consideration that part of the error is due to deviation from the ideal slender beam geometry.

In order to compare the relative advantages of the two types of spring, in figure 7 the calculated and simulated ratios between the corresponding spring constants are shown. To allow this comparison, the longer elements of the two springs (l_o for classic, l_p for rotated springs) were made equal. The ratios for K_x and K_{δ_y} are almost coincident, while for the other two constants a significant deviation is observed for high thickness. Nonetheless, the behavior as a function of the length is similar. This means that, at least for small thicknesses, the analytical formulae can be used to compare the springs' performance and they are an effective help to the designer in the choice of the best structure.

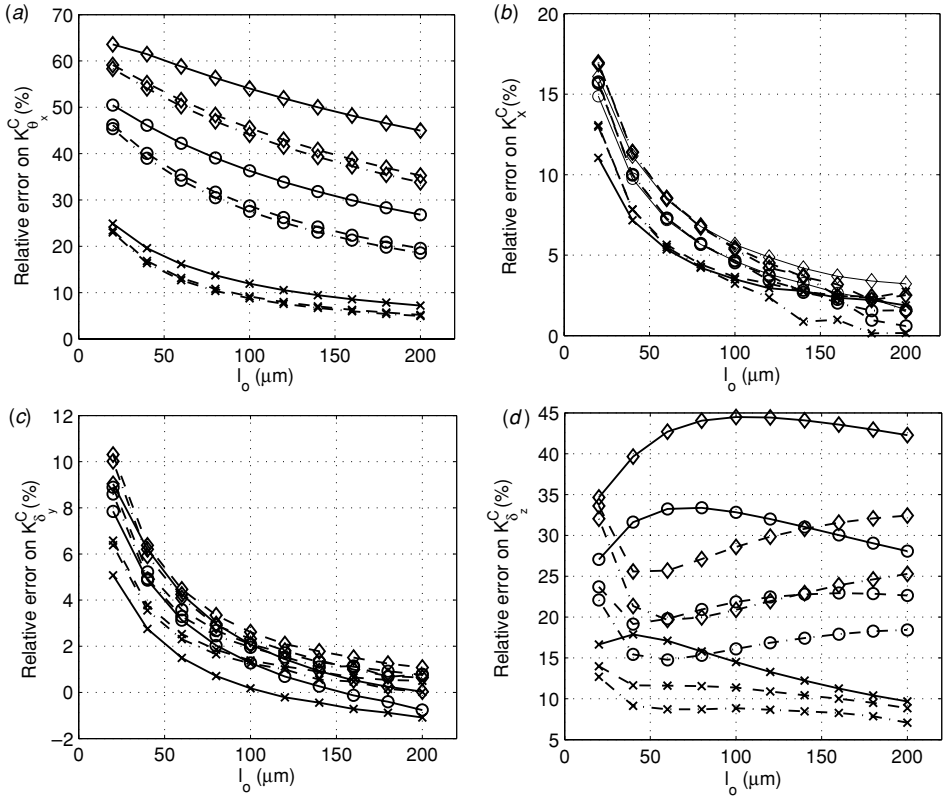

Figure 5. Relative error on the spring constants of the classic serpentine springs: $K^{\mathrm{C}}_{\theta_x}$ (*a*); K^{C}_{x} (*b*); $K^{\mathrm{C}}_{\delta_y}$ (*c*); $K^{\mathrm{C}}_{\delta_z}$ (*d*). ——○ $t = 10\ \mu$m, $N = 0$; – – –○ $t = 10\ \mu$m, $N = 3$; — · —○ $t = 10\ \mu$m, $N = 5$; ——◇ $t = 15\ \mu$m, $N = 0$; – – –◇ $t = 15\ \mu$m, $N = 3$; — · —◇ $t = 15\ \mu$m, $N = 5$; —— X $t = 5\ \mu$m, $N = 0$; – – – X $t = 5\ \mu$m, $N = 3$; — · — X $t = 5\ \mu$m, $N = 5$.

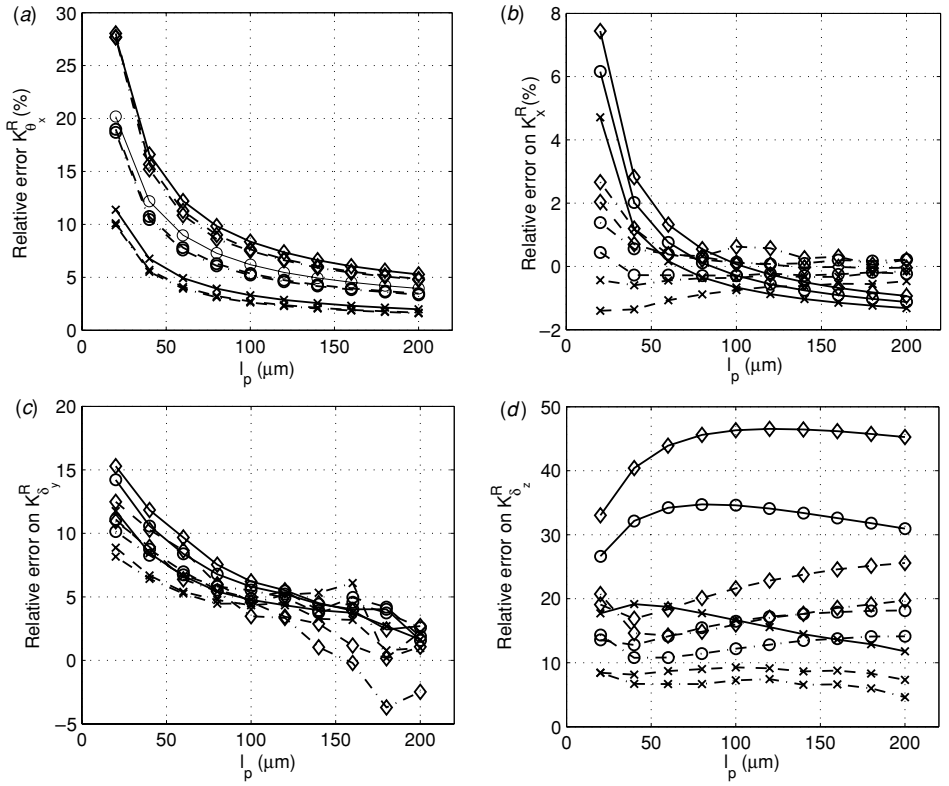

Figure 6. Relative error on the spring constants of the rotated serpentine springs: $K^{\mathrm{R}}_{\theta_x}$ (*a*); K^{R}_{x} (*b*); $K^{\mathrm{R}}_{\delta_y}$ (*c*); $K^{\mathrm{R}}_{\delta_z}$ (*d*). ——○ $t = 10\ \mu$m, $N = 0$; – – –○ $t = 10\ \mu$m, $N = 3$; — · —○ $t = 10\ \mu$m, $N = 5$; ——◇ $t = 15\ \mu$m, $N = 0$; – – –◇ $t = 15\ \mu$m, $N = 3$; — · —◇ $t = 15\ \mu$m, $N = 5$; —— X $t = 5\ \mu$m, $N = 0$; – – – X $t = 5\ \mu$m, $N = 3$; — · — X $t = 5\ \mu$m, $N = 5$.

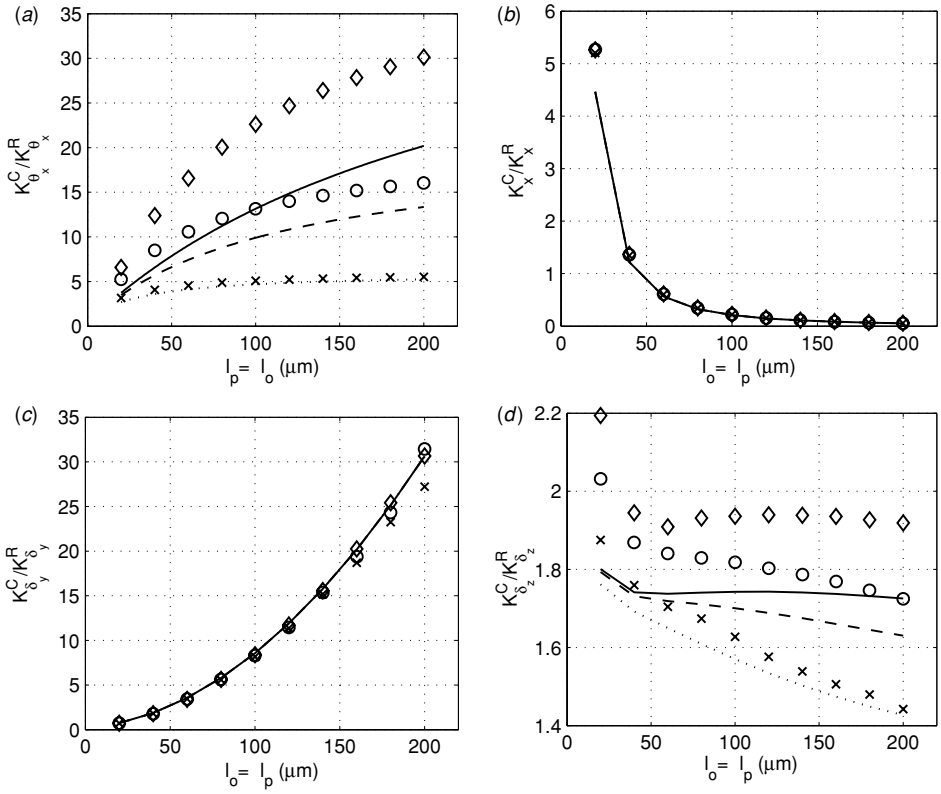

Figure 7. Ratio between the corresponding spring constants of the two structures ($N = 3$). From simulations: ◊ $t = 15$ μm; ○ $t = 10$ μm; X $t = 5$ μm. From analytical formulae: —— $t = 15$ μm; – – – $t = 10$ μm; · · · · · · $t = 5$ μm.

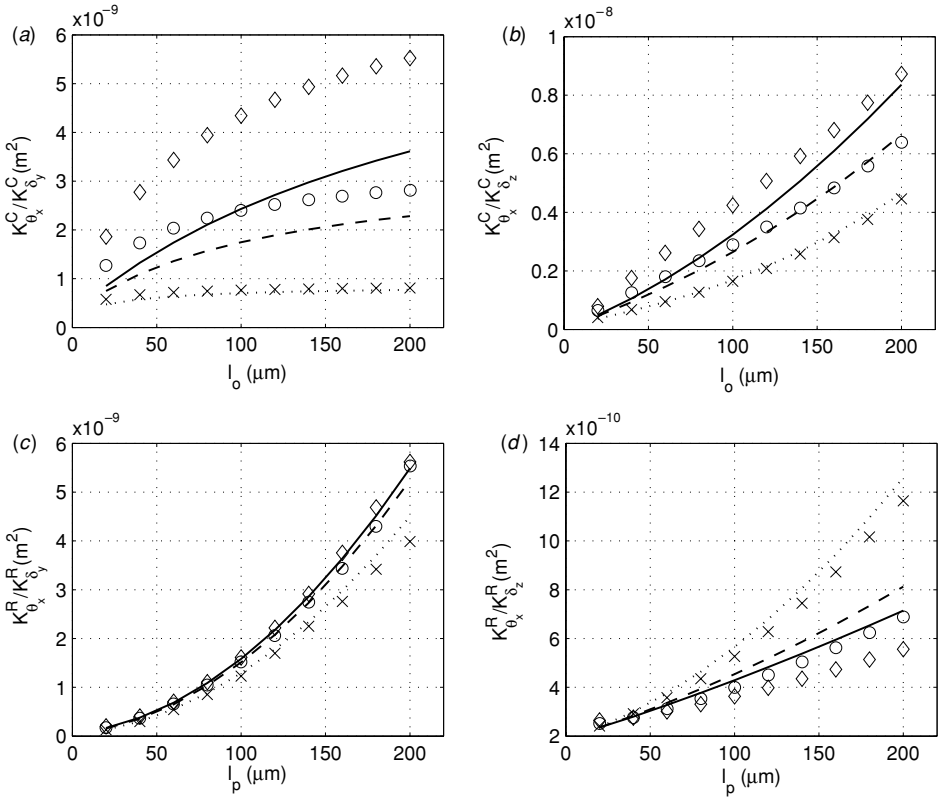

Figure 8. Ratios $K^C_{\theta_x}/K^C_{\delta_y}$ (*a*); $K^C_{\theta_x}/K^C_{\delta_z}$ (*b*); $K^R_{\theta_x}/K^R_{\delta_y}$ (*c*); $K^R_{\theta_x}/K^R_{\delta_z}$ (*d*) with $N = 3$. From simulations: ◊ $t = 15$ μm; ○ $t = 10$ μm; X $t = 5$ μm. From analytical formulae: —— $t = 15$ μm; – – – $t = 10$ μm; · · · · · · $t = 5$ μm.

With the help of the data in figure 7, a comparison of the two designs in torsional applications can be carried out as well. In particular, the torsional spring constant for rotated springs is much smaller than for classic springs, especially for high thickness, as expected. Another measure of the suitability of rotated springs for torsional applications is given by the ratios between K_θ and the other constants, ratios which should be as small as possible to reduce the impact of parasitic resonant modes (i.e. to keep these modes at high frequency). Sample ratios for classic and rotated springs are shown in figure 8. The ratios with respect to K_{δ_y} are of the same order of magnitude for the two designs, while for K_{δ_z} the rotated spring behaves much better than the other (by two orders of magnitude), confirming quantitatively the advantages of the latter design for torsional springs.

Another important piece of information contained in figure 7 is that the classic serpentine springs are, by contrast, a much better choice when they are used as elastic elements in the x-direction, because their K_x is much smaller. This explains why they are commonly used for linear, in-plane actuators/ sensors [1, 7], which probably are, to date, the majority of developed MEMS devices.

5. Conclusions

In this paper we showed an analytical approach to evaluate the spring constants of serpentine springs, useful in microstructures design. Two kinds of serpentine springs were analyzed: one with classic shape and another with rotated serpentine shape. FEM simulations were used to check the analytical formulae and it was shown that the results are in accordance with the theory in the range of validity of the beam approximation. It was found that the analytical formulae are useful to compare the performances of the two kinds of springs. It was also verified that the rotated serpentine springs are more suitable for torsional applications, especially for high thickness of the structural layer.

Appendix A. Unit-load method

The spring constants are deduced from a set of linear equations obtained by using the principle of virtual work with the unit-load method. The principle of virtual work states that if a deformable structure in equilibrium under the action of a system of loads is given a small virtual deformation, then the virtual work done by the external forces (or loads) equals the virtual work done by the internal forces (or stress resultants) [10]. Two loading systems must be considered when using the unit-load method to find the displacement of a structure. The first system consists of the actual loads, while the second consists of a unit load acting alone on the structure. The unit-load is a dummy load that is introduced for the purpose of calculating the displacement Δ of the structure due to the actual loads. The unit load must correspond to the desired displacement Δ. A load that corresponds to a displacement is a load that acts on the structure at the point where the displacement is to be determined and has its positive direction in the same direction as a positive displacement.

After the application of the unit-load and the use of the principle of virtual work, the following equation is obtained[4] [10]:

$$\left.\begin{matrix} 1\cdot\Delta \\ 1\cdot\phi \end{matrix}\right\} = \int \frac{N_\mathrm{U}N_\mathrm{L}}{EA}\,\mathrm{d}x + \int \frac{M_\mathrm{U}M_\mathrm{L}}{EI}\,\mathrm{d}x + \int \frac{T_\mathrm{U}T_\mathrm{L}}{EJ}\,\mathrm{d}x \qquad \text{(A.1)}$$

N_L, M_L and T_L are the axial force, bending moment and twisting couple caused by the actual loads, respectively, while N_U, M_U and T_U are produced by the unit-load, and have the dimensions of force or moments per unit of the applied unit-load; E is the Young modulus and G the shear modulus, which is equal to $E/(2(1+\nu))$, where ν is the Poisson ratio; A is the cross-section of the beam, I is the moment of inertia of the section and J is the cross-sectional torsion factor. This equation can be used to find the displacement at any point of a structure when the material is linearly elastic.

Appendix B. Calculation of the spring constants

B.1. Torsional spring constant K_{θ_x}

To measure the torsional spring constant we apply a torsion moment M_x and we calculate the rotation by using the unit-load method. For the classical serpentine springs, the following relation is obtained:

$$1\cdot\theta_x = \sum_{\text{beams}} \left(\int_0^{l_\text{beam}} \frac{T_\mathrm{L}T_\mathrm{U}}{GJ}\,\mathrm{d}x + \int_0^{l_\text{beam}} \frac{M_\mathrm{L}M_\mathrm{U}}{EI}\,\mathrm{d}x \right). \qquad \text{(B.1)}$$

The torques and the moments caused by the loads (actual and dummy) are derived and substituted in equation (B.1). In order to make their evaluation easier, for each beam a local system of reference with its x-axis along the central axis is defined. Hence, after the derivation of a free-body diagram, for the classical serpentine spring the following relation is obtained:

$$\begin{aligned}\theta_x = {} & \int_0^{l_\mathrm{p}} \frac{M_x}{GJ_\mathrm{p}}\,\mathrm{d}x + \int_0^{\frac{l_\mathrm{o}}{2}} \frac{M_x}{EI_{y_\mathrm{o}}}\,\mathrm{d}x + \int_0^{l_\mathrm{p}} \frac{M_x}{GJ_\mathrm{p}}\,\mathrm{d}x \\ & + \int_0^{l_\mathrm{o}} \frac{M_x}{EI_{y_\mathrm{o}}}\,\mathrm{d}x + \int_0^{l_\mathrm{p}} \frac{M_x}{GJ_\mathrm{p}}\,\mathrm{d}x + \sum_{i=1}^{N} \left[\int_0^{l_\mathrm{o}} \frac{M_x}{EI_{y_\mathrm{o}}}\,\mathrm{d}x \right. \\ & \left. + \int_0^{l_\mathrm{p}} \frac{M_x}{GJ_\mathrm{p}}\,\mathrm{d}x + \int_0^{l_\mathrm{o}} \frac{M_x}{EI_{y_\mathrm{o}}}\,\mathrm{d}x + \int_0^{l_\mathrm{p}} \frac{M_x}{GJ_0}\,\mathrm{d}x \right] \\ & + \int_0^{\frac{l_\mathrm{o}}{2}} \frac{M_x}{EI_{y_\mathrm{o}}}\,\mathrm{d}x + \int_0^{l_\mathrm{p}} \frac{M_x}{GJ_\mathrm{p}}\,\mathrm{d}x. \end{aligned} \qquad \text{(B.2)}$$

The moment of inertia I_{y_o} and the torsion factor J_p for a beam with rectangular cross-section are [10]:

$$I_{y_\mathrm{o}} = \frac{w_\mathrm{o}t^3}{12} \qquad \text{(B.3)}$$

$$J_\mathrm{p} = \frac{tw_\mathrm{p}^3}{3}\left(1 - \frac{192w_\mathrm{p}}{\pi^5 t}\sum_{i=1,3,5,\ldots}\frac{1}{i^5}\tanh\left(\frac{\mathrm{i}\pi t}{2w_\mathrm{p}}\right)\right). \qquad \text{(B.4)}$$

Simplifying equation (B.2), the following equation is obtained:

$$\theta_x = M_x\left[\frac{2(N+1)}{EI_{y_\mathrm{o}}}l_\mathrm{o} + \frac{2(N+2)}{GJ_\mathrm{p}}l_\mathrm{p}\right]. \qquad \text{(B.5)}$$

[4] Equation (A.1) does not take into account shear deformations. If they are not negligible it is necessary to add the term $\int f_\mathrm{s}\frac{V_\mathrm{U}V_\mathrm{L}}{GA}\,\mathrm{d}x$ to its RHS, where V_L and V_U are the shear forces produced by the actual and dummy load and f_s is the *shear factor* [10].

From equation (B.5) we calculate $K^{\mathrm{C}}_{\theta_x} = M_x/\theta_x$, the torsional spring constant of the classic serpentine spring. Not surprisingly, the result is equal to the series of the spring constant of each element of which the spring is constituted:

$$K^{\mathrm{C}}_{\theta_x} = \left[\frac{2(N+1)}{EI_{y_\mathrm{o}}} l_\mathrm{o} + \frac{2(N+2)}{GJ_\mathrm{p}} l_\mathrm{p}\right]^{-1}. \tag{B.6}$$

In most applications, $l_\mathrm{o} \gg l_\mathrm{p}$ and/or $w_\mathrm{p} \gg w_\mathrm{o}$ are verified, which is equivalent to neglecting the terms relative to the parallel elements because they are much shorter and/or wider than the others, and thus can be considered not deformed. In this case, equation (B.6) reduces to

$$K^{\mathrm{C}}_{\theta_x} \simeq \frac{EI_{y_\mathrm{o}}}{2(N+1)l_\mathrm{o}}. \tag{B.7}$$

We consider the spring with the rotated serpentine and we apply the same method obtaining the following relation:

$$\theta_x = M_x \left[\frac{4(N+1)}{EI_{y_\mathrm{o}}} l_\mathrm{o} + \frac{(2N+3)l_\mathrm{p} + 2d_\mathrm{p} + l_\mathrm{ini} + l_\mathrm{fin}}{GJ_\mathrm{p}}\right]. \tag{B.8}$$

Again we note that the overall spring constant equals that of the series of each element:

$$K^{\mathrm{R}}_{\theta_x} = \left[\frac{4(N+1)}{EI_{y_\mathrm{o}}} l_\mathrm{o} + \frac{(2N+3)l_\mathrm{p} + 2d_\mathrm{p} + l_\mathrm{ini} + l_\mathrm{fin}}{GJ_\mathrm{p}}\right]^{-1}. \tag{B.9}$$

When $l_\mathrm{p} \gg l_\mathrm{o}, l_\mathrm{ini}, l_{\mathrm{fin},d_\mathrm{p}}$ or $w_\mathrm{o} \gg w_\mathrm{p}$ the equation reduces to

$$K^{\mathrm{R}}_{\theta_x} \simeq \frac{GJ_\mathrm{p}}{(2N+3)l_\mathrm{p}}. \tag{B.10}$$

B.2. Spring constant K_x

We use the principle of virtual work by applying an exploratory load along the x-axis. We obtain for the classic serpentine springs:

$$K^{\mathrm{C}}_x = \left[\frac{(N+1)l_\mathrm{o}^3}{6EI_{z_\mathrm{o}}} + \frac{(N+1)l_\mathrm{o}^2 l_\mathrm{p}}{2EI_{z_\mathrm{p}}}\right]^{-1}. \tag{B.11}$$

Again, if $l_\mathrm{o} \gg l_\mathrm{p}$:

$$K^{\mathrm{C}}_x \simeq \frac{6EI_{z_\mathrm{o}}}{(N+1)l_\mathrm{o}^3}. \tag{B.12}$$

For the rotated serpentine spring the following spring constant is calculated:

$$K^{\mathrm{R}}_x = \left[\frac{(4((N+1)l_\mathrm{o})^3}{3EI_{z_\mathrm{o}}} + \frac{(2N^3+9N^2+13N^2+6)l_\mathrm{p} + 6(N+1)d_\mathrm{p}}{3EI_{z_\mathrm{p}}} l_\mathrm{o}^2\right]^{-1}. \tag{B.13}$$

Again, if $l_\mathrm{p} \gg l_\mathrm{o}, d_\mathrm{p}$:

$$K^{\mathrm{R}}_x \simeq \frac{3EI_{z_\mathrm{p}}}{\left(2N^3+9N^2+13N+6\right) l_\mathrm{p} l_\mathrm{o}^2}. \tag{B.14}$$

B.3. Spring constant K_{δ_y} for the classic serpentine springs with guided end

This is a classical *iperstatic* problem which can be addressed by selecting one of the constraints and solving two cases: one with the same load system without the constraint (case (1)), and one where only the unknown reaction due to the excluded constraint, and not the applied loads, is considered (case (2)). The additional unknown, represented by the reaction, is computed by imposing a condition of congruence between the displacement (or rotation) in the direction of the excluded costraints. It is then possible to study a system with the same number of equations and unknowns.

Hence the problem is divided into two parts: in case (1) the relation between θ_{z1} and F_y is calculated:

$$\theta_{z1} = \left(K^{\mathrm{C}}_{\theta_z y}\right)^{-1} F_y. \tag{B.15}$$

In case (2) the relation between θ_{z2} and M_{R_z} is

$$\theta_{z2} = K^{\mathrm{C}-1}_{\theta_z} M_{Rz}. \tag{B.16}$$

The condition of congruence imposes that the sum of the rotation caused by the loads and by the moment of reaction is zero:

$$\theta_{z1} + \theta_{z2} = 0. \tag{B.17}$$

By substituing equations (B.15) and (B.16) into equation (B.17), the moment of the reaction is derived:

$$M_{Rz} = -\frac{K^{\mathrm{C}}_{\theta_z}}{K^{\mathrm{C}}_{\theta_z y}} F_y. \tag{B.18}$$

After these passages the problem is reduced to the calculation of the displacement δ_y when a load F_y and a moment M_{Rx} are applied to a free end of the spring.

$$y = K^{\mathrm{C}-1}_y F_y + K^{\mathrm{C}-1}_{y\theta_z} M_{Rz} = \frac{K^{\mathrm{C}}_{y\theta_z} K^{\mathrm{C}}_{\theta_z y} - K^{\mathrm{C}}_y K^{\mathrm{C}}_{\theta_z}}{K^{\mathrm{C}}_{y\theta_z} K^{\mathrm{C}}_{\theta_z y} K^{\mathrm{C}}_y} F_y. \tag{B.19}$$

Then the spring constant $K^{\mathrm{C}}_{\delta_y}$ is

$$K^{\mathrm{C}}_{\delta_y} = \frac{K^{\mathrm{C}}_{y\theta_z} K^{\mathrm{C}}_{\theta_z y} K^{\mathrm{C}}_y}{K^{\mathrm{C}}_{y\theta_z} K^{\mathrm{C}}_{\theta_z y} - K^{\mathrm{C}}_y K^{\mathrm{C}}_{\theta_z}} \tag{B.20}$$

K^{C}_y, $K^{\mathrm{C}}_{y\theta_z}$, $K^{\mathrm{C}}_{\theta_z y}$ and $K^{\mathrm{C}}_{\theta_z}$ are calculated with the unit-load method:

$$K^{\mathrm{C}}_y = \left[\frac{(2(N+2)l_\mathrm{p})^3}{3EI_{z_\mathrm{p}}} + \frac{(8N^3+36N^2+55N+27)l_\mathrm{p}^2 l_\mathrm{o}}{3EI_{z_\mathrm{o}}}\right]^{-1} \tag{B.21}$$

$$K^{\mathrm{C}}_{y\theta_z} = K^{\mathrm{C}}_{\theta_z y} = \left[\frac{2(N^2+3N+4)l_\mathrm{p} l_\mathrm{o}}{EI_{z_\mathrm{o}}} + \frac{2(N+2)^2 l_\mathrm{p}^2}{EI_{z_\mathrm{p}}}\right]^{-1} \tag{B.22}$$

$$K^{\mathrm{C}}_{\theta_z} = \left[\frac{2(N+2)l_\mathrm{p}}{EI_{z_\mathrm{p}}} + \frac{2(N+1)l_\mathrm{o}}{EI_{z_\mathrm{o}}}\right]^{-1}. \tag{B.23}$$

And, if $l_\mathrm{o} \gg l_\mathrm{p}$:

$$K^{\mathrm{C}}_y \simeq \frac{3EI_{z_\mathrm{o}}}{(8N^3+36N^2+55N+27)l_\mathrm{p}^2 l_\mathrm{o}} \tag{B.24}$$

$$K^{\mathrm{C}}_{y\theta_z} = K^{\mathrm{C}}_{\theta_z y} = \frac{EI_{z_\mathrm{o}}}{2(N^2+3N+2)l_\mathrm{p}l_\mathrm{o}} \tag{B.25}$$

$$K^{\mathrm{C}}_{\theta_z} \simeq \frac{EI_{z_\mathrm{o}}}{2(N+1)l_\mathrm{o}}. \tag{B.26}$$

By substituting expressions (B.24), (B.25) and (B.26) into equation (B.20), the approximate equation valid for $l_\mathrm{o} \gg l_\mathrm{p}$ is deduced:

$$K^{\mathrm{C}}_{\delta_y} \simeq \frac{3EI_{z_\mathrm{o}}(N+1)}{(12N^4+64N^3+130N^2+116N+38)l_\mathrm{p}^2 l_\mathrm{o}}. \tag{B.27}$$

B.4. Spring constant $K^{\mathrm{C}}_{\delta_z}$ for the classic serpentine spring

Similarly to $K^{\mathrm{C}}_{\delta_y}$ in appendix B.3, the spring constant $K^{\mathrm{C}}_{\delta_z}$ is calculated with the following expression:

$$K^{\mathrm{C}}_{\delta_z} = \frac{K^{\mathrm{C}}_{z\theta_y} K^{\mathrm{C}}_{\theta_y z} K^{\mathrm{C}}_{z}}{K^{\mathrm{C}}_{z\theta_y} K^{\mathrm{C}}_{\theta_y z} - K^{\mathrm{C}}_{z} K^{\mathrm{C}}_{\theta_y}} \tag{B.28}$$

K^{C}_{z}, $K^{\mathrm{C}}_{\theta_y z}$, $K^{\mathrm{C}}_{z\theta_y}$ and $K^{\mathrm{C}}_{\theta_y}$ are calculated with the unit-load method:

$$K^{\mathrm{C}}_{z} = \left[\frac{(2(N+2)l_\mathrm{p})^3}{3EI_{y_\mathrm{p}}} + \frac{(N+1)(l_\mathrm{o})^3}{6EI_{y_\mathrm{o}}} + \frac{(N+1)(l_\mathrm{o})^2 l_\mathrm{p}}{GJ_\mathrm{p}} + \frac{(8N^3+36N^2+55N+27)l_\mathrm{p}^2 l_\mathrm{o}}{3GJ_\mathrm{o}}\right]^{-1} \tag{B.29}$$

$$K^{\mathrm{C}}_{\theta_y z} = K^{\mathrm{C}}_{z\theta_y} = \left[\frac{2(N^2+3N+2)l_\mathrm{p}l_\mathrm{o}}{GJ_\mathrm{o}} + \frac{2(N+2)^2 l_\mathrm{p}^2}{EI_{y_\mathrm{p}}}\right]^{-1} \tag{B.30}$$

$$K^{\mathrm{C}}_{\theta_y} = \left[\frac{2(N+2)l_\mathrm{p}}{EI_{y_\mathrm{p}}} + \frac{2(N+1)l_\mathrm{o}}{GJ_\mathrm{o}}\right]^{-1}. \tag{B.31}$$

For $l_\mathrm{o} \gg l_\mathrm{p}$ it is possible to approximate equations (B.30) and (B.31):

$$K^{\mathrm{C}}_{\theta_y z} \simeq \frac{GJ_\mathrm{o}}{2(N^2+3N+2)l_\mathrm{p}l_\mathrm{o}} \tag{B.32}$$

$$K^{\mathrm{C}}_{\theta_y} \simeq \frac{GJ_\mathrm{o}}{2(N+1)l_\mathrm{o}}. \tag{B.33}$$

By supposing $l_\mathrm{o} \gg l_\mathrm{p}$ and high N, equation (B.29) is simplified in

$$K^{\mathrm{C}}_{z} \simeq \left[\frac{(N+1)l_\mathrm{o}^3}{6EI_{y_\mathrm{o}}} + \frac{(8N^3+36N^2+55N+27)l_\mathrm{p}^2 l_\mathrm{o}}{3GJ_\mathrm{o}}\right]^{-1}. \tag{B.34}$$

By substituting the approximate expressions (B.32), (B.33) and (B.34) into (B.28):

$$K^{\mathrm{C}}_{\delta_z} \simeq \frac{6EI_{y_\mathrm{o}}GJ_\mathrm{o}}{(N+1)l_\mathrm{o}^3 GJ_\mathrm{o} + (16N^3+36N^2+43N+3)l_\mathrm{p}^2 l_\mathrm{o} EI_{y_\mathrm{o}}}. \tag{B.35}$$

B.5. Spring constant K_{δ_y} for the rotated serpentine spring

By applying the method described in appendix B.3, K_{δ_y}, the ratio between F_y and δ_y in the condition of the guided end along the y-axis (figure 4), is calculated:

$$K^{\mathrm{R}}_{\delta_y} = \frac{K^{\mathrm{R}}_{y\theta_z} K^{\mathrm{R}}_{\theta_z y} K^{\mathrm{R}}_{y}}{K^{\mathrm{R}}_{y\theta_z} K^{\mathrm{R}}_{\theta_z y} - K^{\mathrm{R}}_{y} K^{\mathrm{R}}_{\theta_z}} \tag{B.36}$$

K^{R}_{y}, $K^{\mathrm{R}}_{\theta_z y}$, $K^{\mathrm{R}}_{y\theta_z}$ and $K^{\mathrm{R}}_{\theta_z}$ are calculated with the unit-load method:

$$K^{\mathrm{R}}_{y} = \left[\frac{(N+1)l_\mathrm{o}\left(l_\mathrm{fin}^2 + (l_\mathrm{fin}+d_\mathrm{p})^2 + (l_\mathrm{fin}+l_\mathrm{p}+d_\mathrm{p})^2 + (l_\mathrm{fin}+2d_\mathrm{p}+l_\mathrm{p})^2\right)}{EI_{z_\mathrm{o}}} + \frac{(2(N+1)((l_\mathrm{fin}+l_\mathrm{p}+d_\mathrm{p})^3 - (l_\mathrm{fin}+d_\mathrm{p})^3)}{3EI_{z_\mathrm{p}}} + \frac{(l_\mathrm{ini}+l_\mathrm{fin}+l_\mathrm{p}+2d_\mathrm{p})^3}{3EI_{z_\mathrm{p}}}\right]^{-1} \tag{B.37}$$

$$K^{\mathrm{R}}_{\theta_z y} = K^{\mathrm{R}}_{y\theta_z} = \left[\frac{2(N+1)l_\mathrm{p}(l_\mathrm{p}+2l_\mathrm{fin}+2d_\mathrm{p}) + (l_\mathrm{ini}+l_\mathrm{fin}+l_\mathrm{p}+2d_\mathrm{p})^2}{2EI_{z_\mathrm{p}}} + \frac{(N+1)l_\mathrm{o}(4l_\mathrm{fin}+4d_\mathrm{p}+2l_\mathrm{p})}{EI_{z_\mathrm{o}}}\right]^{-1} \tag{B.38}$$

$$K^{\mathrm{R}}_{\theta_z} = \left[\frac{(2N+3)l_\mathrm{p}+2d_\mathrm{p}+l_\mathrm{ini}+l_\mathrm{fin}}{EI_{z_\mathrm{p}}} + \frac{4(N+1)l_\mathrm{o}}{EI_{z_\mathrm{o}}}\right]^{-1}. \tag{B.39}$$

For $l_\mathrm{p} \gg l_\mathrm{o}, l_\mathrm{ini}, l_\mathrm{fin}, d_\mathrm{p}$:

$$K^{\mathrm{R}}_{y} \simeq \frac{3EI_{z_\mathrm{p}}}{(2N+3)l_\mathrm{p}^3} \tag{B.40}$$

$$K^{\mathrm{R}}_{\theta_y z} = \frac{2EI_{z_\mathrm{p}}}{(2N+3)l_\mathrm{p}^2} \tag{B.41}$$

$$K^{\mathrm{R}}_{\theta_z} \simeq \frac{EI_{z_\mathrm{p}}}{(2N+3)l_\mathrm{p}}. \tag{B.42}$$

By substituting the approximate expressions of (B.40), (B.41) and (B.42) into (B.36):

$$K^{\mathrm{R}}_{\delta_y} \simeq \frac{12EI_{z_\mathrm{p}}}{(2N+3)l_\mathrm{p}^3}. \tag{B.43}$$

B.6. Spring constant K_{δ_z} for the rotated serpentine spring

We define $K^{\mathrm{R}}_{\delta_z}$ as the ratio between F_z and δ_z in the condition of the guided end along the z-axis (figure 4). With the method in appendix B.3, the following expression is deduced:

$$K^{\mathrm{R}}_{\delta_z} = \frac{K^{\mathrm{R}}_{z\theta_y} K^{\mathrm{R}}_{\theta_y z} K^{\mathrm{R}}_{z}}{K^{\mathrm{R}}_{z\theta_y} K^{\mathrm{R}}_{\theta_y z} - K^{\mathrm{R}}_{z} K^{\mathrm{R}}_{\theta_y}} \tag{B.44}$$

K^{R}_{z}, $K^{\mathrm{R}}_{\theta_y z}$, $K^{\mathrm{R}}_{z\theta_y}$ and $K^{\mathrm{R}}_{\theta_y}$ are calculated with the unit-load method:

$$K^{\mathrm{R}}_{z} = \left[\frac{((2N^3+9N^2+13N+6)l_\mathrm{p}+6d_\mathrm{p}(N+1)^2)l_\mathrm{o}^2}{3GJ_\mathrm{p}} + \frac{4((N+1)l_\mathrm{o})^3}{3EI_{y_\mathrm{o}}} + \frac{2(N+1)((l_\mathrm{fin}+l_\mathrm{p}+d_\mathrm{p})^3 - (l_\mathrm{fin}+d_\mathrm{p})^3) + (l_\mathrm{ini}+l_\mathrm{fin}+l_\mathrm{p}+2d_\mathrm{p})^3}{3EI_{y_\mathrm{p}}} + \frac{(N+1)\left((l_\mathrm{fin}+l_\mathrm{p}+d_\mathrm{p})^2 + (l_\mathrm{fin}+d_\mathrm{p})^2 + (l_\mathrm{fin}+2d_\mathrm{p}+l_\mathrm{p})^2 + l_\mathrm{fin}^2\right)l_\mathrm{o}}{GJ_\mathrm{o}}\right]^{-1} \tag{B.45}$$

$$K^{\mathrm{R}}_{\theta_y z} = K^{\mathrm{R}}_{z\theta_y} = \left[\frac{(l_{\mathrm{ini}} + l_{\mathrm{fin}} + l_{\mathrm{p}} + 2d_{\mathrm{p}})^2}{2EI_{y_{\mathrm{p}}}} + \frac{(2N+2)((l_{\mathrm{fin}} + l_{\mathrm{p}} + d_{\mathrm{p}})^2 - (l_{\mathrm{fin}} + d_{\mathrm{p}})^2)}{2EI_{y_{\mathrm{p}}}} + \frac{(N+1)(4l_{\mathrm{fin}} + 4d_{\mathrm{p}} + 2l_{\mathrm{p}})l_{\mathrm{o}}}{GJ_{\mathrm{o}}} \right]^{-1} \tag{B.46}$$

$$K^{\mathrm{R}}_{\theta_y} = \left[\frac{(2N+3)l_{\mathrm{p}} + 2d_{\mathrm{p}} + l_{\mathrm{ini}} + l_{\mathrm{fin}}}{EI_{y_{\mathrm{p}}}} + \frac{4(N+1)l_{\mathrm{o}}}{GJ_{\mathrm{o}}} \right]^{-1} \tag{B.47}$$

For $l_{\mathrm{p}} \gg l_{\mathrm{o}}, l_{\mathrm{ini}}, l_{\mathrm{fin}}, d_{\mathrm{p}}$:

$$K^{\mathrm{R}}_{\theta_y z} = \frac{2EI_{y_{\mathrm{p}}}}{(2N+3)l_{\mathrm{p}}^2} \tag{B.48}$$

$$K^{\mathrm{R}}_{\theta_y} \simeq \frac{EI_{y_{\mathrm{p}}}}{(2N+3)l_{\mathrm{p}}}. \tag{B.49}$$

For $l_{\mathrm{p}} \gg l_{\mathrm{o}}, l_{\mathrm{ini}}, l_{\mathrm{fin}}, d_{\mathrm{p}}$ and high N:

$$K^{\mathrm{R}}_{z} \simeq \left[\frac{(2N+3)l_{\mathrm{p}}^3}{3EI_{y_{\mathrm{p}}}} + \frac{(2N^3 + 9N^2 + 13N + 6)l_{\mathrm{p}}l_{\mathrm{o}}^2}{3GJ_{\mathrm{p}}} \right]^{-1}. \tag{B.50}$$

By substituting equations (B.48), (B.49) and (B.50) into (B.44), the following expression for K_{δ_z} is obtained:

$$K^{\mathrm{R}}_{\delta_z} \simeq \frac{12EI_{y_{\mathrm{p}}}GJ_{\mathrm{p}}}{(2N+3)l_{\mathrm{p}}^3 GJ_{\mathrm{p}} + 4(2N^3 + 9N^2 + 13N + 6)l_{\mathrm{p}}l_{\mathrm{o}}^2 EI_{y_{\mathrm{p}}}} \tag{B.51}$$

If l_{p} is high and N is low, the following simplified relation is obtained:

$$K^{\mathrm{R}}_{\delta_z} \simeq \frac{12EI_{y_{\mathrm{p}}}}{(2N+3)l_{\mathrm{p}}^3}. \tag{B.52}$$

This relation appears to be useful in spring design, and is empirically deduced in [11]; however, our analysis shows that equation (B.52) is a good approximation of equation (B.44) only for high values of the length l_{p} and very low l_{o} and N.

References

[1] Fedder G 1994 Simulations of microelectromechanical systems *PhD Thesis* University of California at Berkeley pp 85–6

[2] Tang W C 1990 Electrostatic comb drive for resonant sensor and actuator applications *PhD Thesis* Department of Electrical Engineering and Computer Science, University of California at Berkeley

[3] Tang W C, Nguyen H and Howe R T 1989 Laterally driven polysilicon resonant microstructures *Proc. IEEE Micro Electro Mechanical Systems Workshop (Salt Lake City, UT)* pp 53–9

[4] Ford J E, Aksyuk V A, Bishop D J and Walker J A 1999 Wavelength add-drop switching using tilting micromirrors *J. Lightwave Technol.* **17** 904–11

[5] Brennen R, Pisano A and Tang W C 1990 Multiple mode micromechanical resonators *Proc. IEEE Micro Electro Mechanical Systems Workshop* pp 9–14

[6] Hao Z, Wingfield B, Whitley M, Brooks J and Hammer J A 2003 A design methodology for a bulk-micromachined two-dimensional electrostatic micromirror *J. Microelectromech. Syst.* **12** 692–701

[7] Galayko D, Kaiser A, Buchaillot L, Legrand B, Collard D and Combi C 2003 Design, realization and testing of micro-mechanical resonators in thick-film silicon technology with postprocess electrode-to-resonator gap reduction *J. Micromech. Microeng.* **13** 134–40

[8] http://www.europractice.bosch.com/en/start/index.htm

[9] Aksyuk V A, Simon M E, Pardo F, Arney S, Lopez D and Villanueva A 2002 Optical MEMS design for telecommunications applications *Solid-State Sensor, Actuator and Microsystems Workshop (Hilton Head Island, SC, 2–6 June 2002)*

[10] Gere J M and Timoshenko S P 1991 *Mechanics of Materials* 3rd edn (London: Chapman and Hall)

[11] Xiao Z, Peng W and Farmer K R 2003 Analytical behavior of rectangular electrostatic torsion actuators with nonlinear spring bending *J. Microelectromech. Syst.* **12** 929–36

[12] Iyer S, Zhou Y and Mukherjee T 1999 Analytical modeling of cross-axis coupling in micromechanical springs *Technical Proc. 1999 Int. Conf. on Modeling and Simulation of Microsystems* pp 632–5